The Astrophysical Journal, 743:52 (10pp), 2011 December 10 doi:10.1088/0004-637X/743/1/52

TESTING PHOTOMETRIC DIAGNOSTICS FOR THE DYNAMICAL STATE AND POSSIBLE INTERMEDIATE-MASS BLACK HOLE PRESENCE IN GLOBULAR CLUSTERS

Eva Noyola[1,2,3] and Holger Baumgardt[4,5]

[1] Max-Planck-Institut for Extraterrestrial Physics, Giessenbachstrasse, 85748 Garching, Germany; noyola@astro.unam.mx

[2] Universitäts-Sterwarte München, Scheinerstrasse 1, 81679 Munich, Germany

[3] Instituto de Astronomia, Universidad Nacional Autónoma de México, A.P. 70-264, 04510, México

[4] Argelander Institute for Astronomy, University of Bonn, Auf dem Hügel 71, 53121 Bonn, Germany; h.baumgardt@uq.edu.au

[5] School of Mathematics and Physics, The University of Queensland, Brisbane, QLD 4072, Australia

Received 2009 July 14; accepted 2011 August 18; published 2011 November 22

ABSTRACT

Surface photometry is a necessary tool to establish the dynamical state of star clusters. We produce realistic *HST*-like images from *N*-body models of star clusters with and without central intermediate-mass black holes (IMBHs) in order to measure their surface brightness profiles. The models contain ∼600,000 individual stars, black holes of various masses between 0% and 2% of the total mass, and are evolved for Hubble time. We measure surface brightness and star count profiles for every constructed image in order to test the effect of IMBHs on the central logarithmic slope, the core radius, and the half-light radius. We use these quantities to test diagnostic tools for the presence of central black holes using photometry. We find that the only models that show central shallow cusps with logarithmic slopes between −0.1 and −0.4 are those containing central black holes. Thus, the central logarithmic slope seems to be a good way to choose clusters suspected of containing IMBHs. Clusters with steep central cusps can definitely be ruled out to host an IMBH. The measured r_c/r_h ratio has similar values for clusters that have not undergone core-collapse and those containing a central black hole. We note that observed Galactic globular clusters have a larger span of values for central slope and r_c/r_h than our modeled clusters, and suggest possible reasons that could account for this and contribute to improved future models.

Key words: black hole physics – globular clusters: general – techniques: photometric

Online-only material: color figures

1. INTRODUCTION

Surface photometry has often been the initial tool to establish the dynamical state of globular clusters. The fact that the observed radial density of most clusters appears to be well described by King models (King 1966) has been taken as evidence that these clusters are relaxed systems and that their dynamical evolution is dominated by two-body relaxation processes. A natural consequence of two-body relaxation is the onset of core-collapse, where the central density of a star cluster increases, while the core radius decreases (see Section 1.2 of Noyola & Gebhardt 2006 for a detailed description of the process). Some clusters have been identified as having undergone core-collapse. These are cases with very concentrated surface density profiles, showing steep central cusps with a central projected logarithmic slope of ~ -0.7 (Cohn 1980), that depart from King-type cores. About 20% of the Galactic globular cluster population falls into this category (Trager et al. 1995).

Kinematical evidence for core-collapse accompanied by tailored models has been presented for three clusters: M15 (Dull et al. 1997), NGC 6397 (Drukier 1995), and M71 (Drukier et al. 1992). The expected velocity cusp has only been resolved and modeled for M15 (Baumgardt et al. 2003b; McNamara et al. 2004; van den Bosch et al. 2006). NGC 6752 has been considered to be a post-core-collapse cluster by many authors, but different data sets and analysis methods find that it has a small flat central core (Lugger et al. 1995; Ferraro et al. 2003; Noyola & Gebhardt 2006). The size of the core might be consistent with models for gravothermal oscillations (Vesperini & Chernoff 1994). This cluster shows a steep central velocity cusp (Drukier et al. 2003), but no tailored core-collapse model has been created for it.

There are a variety of heating mechanisms that can drive energy into the core of a star cluster, causing it to expand, and thus preventing core-collapse. The effect of binary heating by primordial binaries is the best-studied mechanism to date (Gao et al. 1991; Vesperini & Chernoff 1994), although it has been proposed that most Galactic globular clusters are not yet in the binary-burning phase of evolution (Fregeau 2008). The presence of stellar-mass black holes acting as an energy source has recently been invoked to explain the distribution of core sizes in Large Magellanic Cloud (LMC) and Small Magellanic Cloud (SMC) globular clusters (Mackey et al. 2008). Mass loss by stellar winds during early times of the cluster evolution also contributes to cluster expansion (Baumgardt & Kroupa 2007; Hurley 2007; Bastian et al. 2008), so clusters might expand considerably even if they are born with concentrated configurations. A recently proposed mechanism is velocity kicks imparted during white dwarf formation, which would also act as a heating mechanism for clusters with velocity dispersions of a few km s^{-1} (Davis et al. 2008; Fregeau et al. 2009).

The presence of a central intermediate-mass black hole (IMBH) of 100–10,000 $M_\odot$ is another mechanism that can affect the dynamical evolution of star clusters. Bahcall & Wolf (1976) calculated the shape of the radial density profile for a single-mass star cluster around a massive black hole. They predicted the formation of a steep central cusp with a logarithmic slope of −1.75. Baumgardt et al. (2004a, 2004b) confirmed these results based on direct *N*-body simulations. They also showed that multi-mass clusters with IMBHs are mass-segregated in their centers and that main-sequence stars have cusps that are significantly flatter than −1.75. They found that the IMBHs appear to produce shallow central cusps on the projected density profiles of bright main-sequence stars for

these clusters, with slopes of ~ -0.2, as opposed to steep power laws (Baumgardt et al. 2005). Noyola & Gebhardt (2006, 2007, hereafter called respectively NG06 and NG07) obtained surface brightness profiles from *Hubble Space Telescope* (*HST*) images for Galactic, LMC, SMC, and Fornax dwarf galaxy globular clusters. They found that about 20% of the globular clusters in their sample show central slopes in this intermediate range.

The surface density profile shape can also be affected in the size of its core when a central black hole is present. Trenti et al. (2007) estimated the value of r_c/r_h (ratio of core radius to half-light radius) for *N*-body simulated star clusters containing central black holes. They used a density-averaged radius as a measure for the core radius. They found that the ratio tends to reach values around 0.3 for these cases, while the value is considerably smaller (<0.1) for clusters without black holes. On the other hand, Hurley (2007) finds similarly large r_c/r_h values for *N*-body simulations evolved including 0.5%–10% primordial binaries, but without a central black hole. In this case, the Casertano and Hut method (Casertano & Hut 1985) was used to obtain the three-dimensional core radius. The way in which the core radius was measured from the *N*-body simulations differs between the two results. Recently, Vesperini & Trenti (2010) analyzed direct *N*-body models with and without IMBHs. They found that shallow cusps with logarithmic slopes as steep as -0.3 are present in various models, not only the ones containing black holes. The apparent discrepancies between different models using different analysis techniques stress the importance of performing meaningful measurements on models so they can be properly compared with observational data.

Direct dynamical evidence for the existence of central black holes using velocity dispersion measurements has been put forward for three nearby globular clusters. M15 was the first case (Gerssen et al. 2002, 2003), but alternative models without black holes were also shown to be good fits to the data (Baumgardt et al. 2003b). The latest detailed dynamical measurement and model find non-conclusive evidence for the presence of a central black hole in this cluster (van den Bosch et al. 2006). G1, a large globular cluster in Andromeda, has stronger observational evidence to support the presence of a central black hole, from integrated kinematical measurements (Gebhardt et al. 2003, 2005), as well as from X-ray (Pooley & Rappaport 2006) and radio (Ulvestad et al. 2007) observations, but alternative scenarios have also been presented for this case (Baumgardt et al. 2003c). Omega Centauri is the most recent case for which line-of-sight velocity dispersion measurements appear to support the existence of a central black hole of 40,000 $M_\odot$ (Noyola et al. 2008), but proper motion measurements from *HST* images find different results (Anderson & van der Marel 2010; van der Marel & Anderson 2010). Evidence has also surfaced for IMBHs in extragalactic disk galaxies based on X-ray observations.

Ultraluminous X-ray sources (ULXs) have X-ray luminosities higher than the Eddington limit for a stellar-mass black hole. One of the possible explanations for this emission is that it comes from accretion onto an IMBH. For example, the galaxy M82 contains a ULX source which is believed to host an IMBH based on the absolute brightness of the source (Matsumoto & Tsuru 1999; Matsumoto et al. 2001) and its radio variability (Strohmayer & Mushotzky 2003). The position of the X-ray source appears to coincide with the young dense star cluster MGG-11 (McCrady et al. 2003). There is also the controversial case of the globular cluster RZ 2109 in NGC 4472, which shows the first clear evidence for a star cluster hosting a black hole (Maccarone et al. 2007), but the size of the black hole is still under debate (Zepf et al. 2008). One more interesting object is the X-ray source CXOJ033831.8-352604, associated with a globular cluster in the Fornax elliptical galaxy NGC 1399. Irwin et al. (2010) suggest the emission might come from a tidally disrupted white dwarf around an IMBH.

In this paper, we create synthetic *HST*-like images from *N*-body simulations with and without IMBHs. We measure their surface brightness profiles as we would with observations. We provide an analysis of the detailed shape of central density profiles for these models that helps understand the central state of Galactic globular clusters. We describe the *N*-body models in Section 2, the synthetic images in Section 3, data analysis in Section 4, and discussion in Section 5.

2. *N*-BODY MODELS

It is often challenging to make a direct comparison between the results of *N*-body models and observations because it is hard to take into account the sources of uncertainty of observations. It is complicated to discriminate how much of the information from the models would be available to an observer if the simulated object was in the sky at a realistic distance. With the goal of making more meaningful comparisons, we take the output of *N*-body models and create realistic synthetic images from them.

The simulations used here followed the evolution of star clusters with and without central IMBHs. All star clusters contained 131,072 (128K) stars initially and were simulated with the *N*-body program NBODY4 (Aarseth 1999) using the GRAPE-6 computers at Tokyo University. Stellar evolution was followed using the fitting formula of Hurley et al. (2000), assuming a metallicity of $Z = 0.001$. For most models, the initial density profile was given by a King $W_0 = 7$ configuration but we also include two models that started from a King $W_0 = 5$ configuration. The detailed description of the runs can be found in Baumgardt et al. (2003a, 2005), called BM03 and BMH05, respectively.

Models m1t and m2t are models without IMBHs. The data were taken from the $N = 128$K star runs in BM03b, which assumed a neutron star retention fraction of 10% and a mass range between 0.1 and 15 $M_\odot$, according to a Kroupa (2001) mass function. Model m3t is a new model made for this paper, starting with $N = 128$K stars distributed according to a Kroupa (2001) initial mass function from 0.1 to 100 $M_\odot$, and with an assumed neutron star and stellar black hole retention fraction of 10% (Pfahl et al. 2002a, 2002b). The retention fractions are assumed to be the same for simplicity, since there is still considerable uncertainty about these numbers. This simulation contains stellar-mass black holes with masses up to 25 $M_\odot$ until the stellar-mass black holes have kicked each other out in two- and three-body interactions at about $T = 12$ Gyr. All models without black holes are at a galactocentric distance of 8.5 kpc. Models mb1t–mb4t come from BMH05, in this case the neutron star retention fraction was 15%, and the stellar mass range went from 0.1 to 30 $M_\odot$, assuming the same mass function as for the non-IMBH cases. The models contain IMBHs of masses 0.2%, 0.5%, 1.0%, and 2.0% of the total mass of the star cluster ($M_{\rm TOT}$). If we extrapolate the scaling laws for supermassive black holes in galaxies to the mass regime of globular clusters, the case with $M_\bullet = 0.5\%\ M_{\rm TOT}$ would follow the Magorrian relation (Magorrian et al. 1998). Stars passing close to the IMBH were assumed to be tidally disrupted. We use the Kochanek (1992) formula for the disruption radius.

Table 1
N-body Models

Model	Source	T_e (Gyr)	$M_\bullet/M_{\rm TOT}$ ($M_\odot$)	W_0	Total N 10^3 Stars	Input N 10^3 Stars
m1t1.0	BM03	1.0	...	7	515	342
m1t4.0	BM03	4.0	...	7	474	308
m1t7.0	BM03	7.0	...	7	444	298
m1t9.0	BM03	9.0	...	7	439	294
m1t10.0	BM03	10.0	...	7	401	271
m1t11.0	BM03	11.0	...	7	416	282
m1t12.5	BM03	12.5	...	7	394	267
m1t16.0	BM03	16.0	...	7	354	241
m2t2.0	BM03	2.0	...	5	513	219
m2t6.0	BM03	6.0	...	5	414	220
m2t8.0	BM03	8.0	...	5	361	221
m3t2.0	...	2.0	...	5	507	163
m3t5.0	...	5.0	...	5	587	165
m3t8.0	...	8.0	...	5	529	141
m3t11.0	...	11.0	...	5	560	148
m3t14.0	...	14.0	...	5	567	151
mb1t11.5	BMH05	11.5	0.2%	7	517	239
mb2t11.0	BMH05	11.0	0.5%	7	519	240
mb2t11.5	BMH05	11.5	0.5%	7	517	236
mb2t12.0	BMH05	12.0	0.5%	7	516	233
mb3t11.5	BMH05	11.5	1.0%	7	515	223
mb4t3.0	BMH05	3.0	2.0%	7	520	188
mb4t6.0	BMH05	6.0	2.0%	7	519	159
mb4t9.0	BMH05	9.0	2.0%	7	518	138
mb4t11.0	BMH05	11.0	2.0%	7	518	224
mb4t11.5	BMH05	11.5	2.0%	7	516	220
mb4t12.0	BMH05	12.0	2.0%	7	515	216
mb5t11.3	...	11.3	2.0%	7	516	186
mb5t11.8	...	11.8	2.0%	7	516	184
mb5t12.0	...	12.0	2.0%	7	515	180

We also performed one additional simulation of a star cluster with an IMBH (called mb5t in Table 1). For this simulation we overlayed four snapshots of the mb4t cluster at $T = 11$ Gyr and continued the simulation for 1 Gyr with $N = 508{,}000$ stars. Given the large number of stars, no stacking was necessary for this cluster. We use this model to test if there is any effect from the stacking of close snapshots.

For the non-IMBH models, we created different snapshots in order to investigate the core-collapse evolution. Snapshots were taken at 1.0, 4.0, 7.0, 9.0, 10.0, 11.0, 12.5, and 16.0 Gyr for the m1t case and 2.0, 6.0, and 8.0 Gyr for the m2t case. For the m1t model, core-collapse occurs at 12.5 Gyr, while this happens at $T = 21.3$ Gyr for the m2t model and at $T = 20.5$ for model m3t. For the models containing IMBHs we use snapshots at different evolutionary times, all between 11 and 12 Gyr, except model mb4t, for which we have earlier snapshots. Information extracted from the models include mass, position, V magnitude, and temperature of each star. The details of the created models can be found in Table 1.

Given the initial number of stars and their mass function, stellar evolution, tidal evaporation, and disruption of stars by the IMBH, the final mass of the models is between $15{,}000\,M_\odot$ and $45{,}000\,M_\odot$, which is only about 1%–10% the mass of a typical Milky Way globular cluster. Since the analysis performed in this work requires a large signal in the images, we had to resort to stacking snapshots separated by short periods of time around a given age for every model. For the models without an IMBH, we stack ∼10 snapshots separated by 15 Myr, while for the models containing IMBHs we stack 5 snapshots separated by 5 Myr. The ultimate goal is to have the same number of stars in the central region for every model. Models with IMBHs are not subject to any external tidal forces, while the models without IMBHs are placed on a circular orbit around a Galactic tidal field and therefore undergo a stronger mass loss. In the end, the total number of stars present in our original lists is always around $N \sim 500{,}000$. The total mass for the stacked models is $\sim 220{,}000\ M_{\rm odot}$ for the non-black hole models and $\sim 180{,}000\ M_{\rm odot}$ for models with central black holes. Variations between individual models are under 10%.

The total number of stars for each N-body model is given in Column 6 of Table 1. The number of stars included in the synthetic images is given in Column 7. As explained in detail in Section 3, this constitutes only ∼50% of the original list due to brightness and radius cuts. The modeled clusters are also more extended compared to the Galactic clusters. With the goal of making the modeled clusters look more like dense Milky Way clusters, we also scaled the clusters down in size. We do this by dividing their coordinates by a common factor, which we chose to be a factor of ∼eight for the models without IMBHs and a factor of four for the models with IMBHs. This scales all clusters down to a similar half-light radius (7–10 pc for non-collapsed cases), which is similar to that measured for Galactic globular clusters.

3. CREATING SYNTHETIC IMAGES

Our main goal is to create realistic images from the N-body models in order to perform the same type of analysis that we do on *HST* observations. The quality and size of the images is chosen to match that of the PC chip in WFPC2 or the High Resolution Channel (HRC) in Advanced Camera for Surveys (ACS). In this way, we can make a proper comparison with observed clusters contained on NG06.

The procedure to create images is like the one described in detail in NG06 and NG07. We use DAOPHOT (Stetson 1987) to add stars from a list of positions and magnitudes onto a base image. With the goal of including realistic background noise, we use as a base a WFPC2 image of a sparse field with the few present stars cleanly subtracted. We modify the base image to have a larger number of pixels than the PC chip on WFPC2, and we locate the center of the cluster at the center of the base image. The utilized point-spread function (PSF) is obtained from observed data and it does not include variations across the chip.

Since the center of observed clusters is not known a priori, we made a blind test in which the center of the models was given an arbitrary shift in the three spatial coordinates, and the new center was calculated using the octants method described in detail in NG06. We choose a guess center and a radius, we count the stars present in eight "pie slice" segments defined by the chosen center and radius and we calculate the standard deviation of the eight numbers. Using the same radius, we move to a new guess center and repeat the procedure several times around the initial guess center. In the end, we have a map of center locations and a standard deviation value associated to each of them. We fit a smoothing spline to the resulting surface and find the location of the minimum defined by the grid of guess centers, which we take as the true center. For this procedure, we used every star in the list, which implies using many more stars than the ones that would be available to an observer. Our goal is to test the method for a complete data set, not to test the observed accuracy of the measurement, since this has already been tested in NG06 and NG07. The centers were calculated for three projections

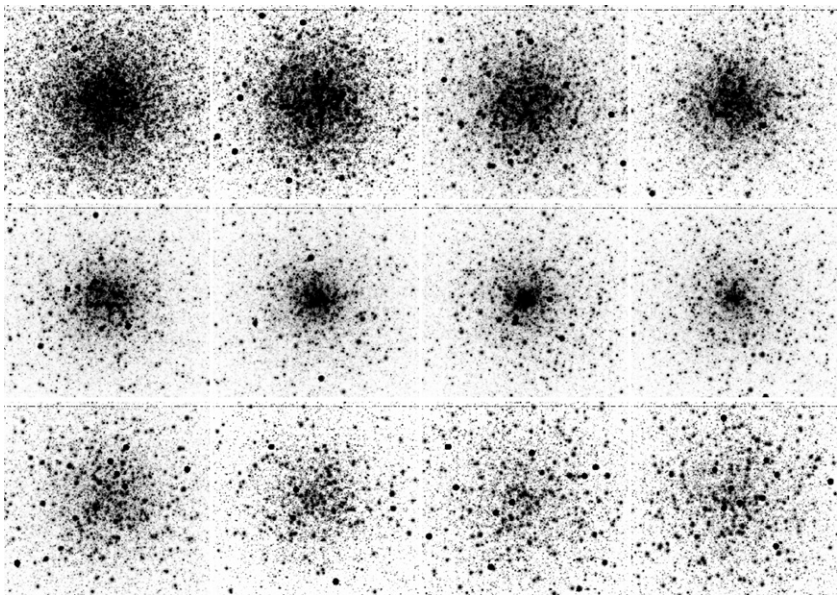

Figure 1. Synthetic images for various *N*-body simulations. The top and middle rows show a cluster without a central IMBH at different evolutionary times of 1.0, 4.0, 7.0, 9.0, 10.0, 11.0, 12.5, and 16.0 Gyr (models m1t1.0–m1t16.0 of Table 1). The bottom row shows clusters containing IMBHs of 0.2%, 0.5%, 1.0%, and 2.0% $M_{\rm TOT}$ (models mb1t11.5, mb2t11.5, mb3t11.5, and mb4t11.5 of Table 1). The evolution toward core-collapse for the non-IMBH case is clearly visible on the images in the upper and middle rows.

on the x–y, x–z, and y–z planes. In the end, we found that the method is able to recover the center with an accuracy of 0.01 pc ($\sim 0.005 r_c$). The tests performed in NG06 yield an error for the observed center location that corresponds to $\sim 0.05 r_c$. In general, the effect of measuring a density profile using the wrong radius is not necessarily to change the central surface brightness slope, but instead, a drop in the central measurement point is created. Seeing such a drop is actually an indication of having the wrong center, Lanzoni et al. (2007) use this fact as a test for correct centering in their work, for example. Despite that drop, the slope of the other points up to the core radius is normally the same as the one using the correct radius. This is clearly seen comparing the profiles for omega Centauri between Noyola et al. (2008) and Anderson & van der Marel (2010). Despite using very different centers, and getting density profiles with different shapes, the slope of the profile between 15″ and the core radius is consistent in both cases.

The next step for making star lists suitable to be turned into images is projecting the stellar coordinates into a two-dimensional distribution in the sky. We need to assume a fiducial distance that will affect both the coordinates and the magnitude of each star. The chosen distance for all cases was 5 kpc, which is on the near end of the distribution of distances for Galactic clusters. We choose this distance since it is adequate for our goal of obtaining high signal-to-noise images. After performing the geometrical projection and applying the distance modulus to the star's magnitudes, bolometric corrections are performed to obtain the V-band luminosity of each star. The correction is done taking into account the star's temperature following the procedure by Hurley et al. (2000). We create synthetic images using DAOPHOT, which has a fiducial zero photometric point of 25 mag, therefore, we eliminate from our list all stars fainter than that. These faint stars constitute ∼20% of the entire list. At 5 kpc distance, 1 pc radius is equivalent to 41.″25. Assuming a pixel scale of 0.″1 per pixel, this is equivalent to ∼412 pixels. Taking into account the extra scaling factor mentioned in Section 2, the synthetic images (1000 pixels on the side) contain stars inside a radius of ∼10 pc for each simulated cluster. Since we are interested in the central structure of the clusters, we choose the image size to include approximately 10 core radii, and we exclude stars outside this radius. The final images end up including ∼50% of the total number of stars in the simulated clusters.

The results for a subset of the models can be seen in Figure 1. For the model without an IMBH, it is clear that the cluster achieves a very concentrated configuration as it evolves toward core-collapse. On the other hand, the clusters containing central IMBHs are less dense and have more extended cores. Once we have the synthetic images, we proceed to analyze them in the same way as we do with observed data.

We count the number of detected stars inside the average core radius for our models. The average detected stellar density in this region is ∼2 stars arcsec^{-2}. For comparison, this is an order of magnitude lower than the central density detected for NGC 6388 by Lanzoni et al. (2007). From the Noyola & Gebhardt (2006) compilation, we located two clusters at different heliocentric distances that have similar central densities to our models: NGC 5634 (30 kpc) and NGC 6541 (7.5 kpc; Harris 1996).

4. SURFACE DENSITY PROFILES

We measure surface density profiles for every synthetic image following the prescription described in detail in NG06. Using various DAOPHOT routines, we find stars and then perform PSF-fitting photometry on them. DAOPHOT allows for the inclusion of noise when adding synthetic stars, therefore, even when we utilize the same PSF used to create the images for our photometric measurements, the subtractions are not perfect and are comparable to those in observed data. We have tested our measurement methods thoroughly using simulated images in NG06 and NG07. We know that we can measure the input centers within ∼1″ for concentrated clusters, therefore, we directly use the known input center for every image when we measure density profiles.

The density profiles are obtained in two different ways: from integrated light and using star counts. A detailed discussion of the pros and cons for each method can be found in

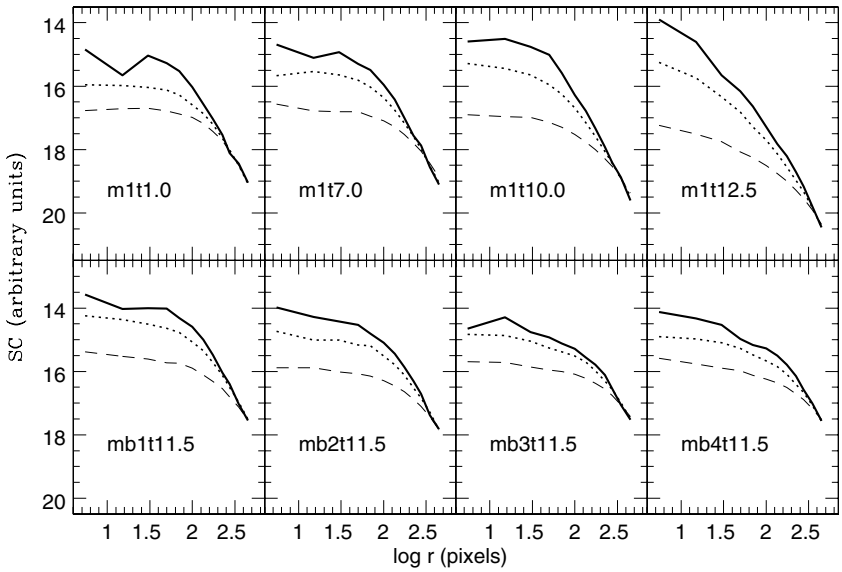

Figure 2. Star count projected density profiles from the input lists, which contain more stars than those detected in the synthetic images. For every case, the magnitude bins are: $V_{\rm mag} < 16$ (solid line), $16 < V_{\rm mag} < 20$ (dotted line), and $V_{\rm mag} > 20$ (dashed line). The top row shows a case without an IMBH at evolutionary times of 1.0, 7.0, 10.0, and 12.5 Gyr (models m1t1.0, m1t7.0, m1t10.0, and m1t12.5). The bottom row shows cases containing IMBHs of 0.2%, 0.5%, 1.0%, and 2.0% $M_{\rm TOT}$ (models mb1t11.5, mb2t11.5, mb3t11.5, and mb4t11.5). The evolution toward core-collapse affects the bright and intermediate bins, but not the faintest one. The presence of an IMBH affects the central slope of brighter bins and the core radius of every stellar group.

Section 2.3 of NG06. For the first method, we use the magnitudes of detected stars to identify the brightest 2%–3%, and we then proceed to mask them by giving them a value that excludes them from the integrated light measurement. For most stars, we assign a masking radius of 3 pixels, which only eliminates the central bright region of stars, not the halo. Occasionally, if very bright stars are present near the center of the cluster, we use a larger radius to mask those. The haloes of the stars do contribute to the total light, but by masking the central part of the PSF disk, one prevents the giant stars from dominating the measurements. Obviously, the "contamination" effect is stronger in the very central regions in cases where there are many giant stars (like in post-core-collapse). In our models, the integrated light follows the input profile very closely even in these cases. Also, Lützgendorf et al. (2011) perform detailed PSF contribution estimations for ACS imaging of NGC 6388. They conclude that the contribution of bright stars after masking the central part of the PSF is under 10% for bins containing 10 pixels or more. Our bins are always larger than that.

The number of detected stars is roughly 10% of the input stars, although it is worth pointing out that about 70% of the input stars are fainter than 20th magnitude. These stars make an important contribution to background light, but they are only detected as individual sources with low efficiency. As expected, the detection efficiency is close to 100% for the brightest stars ($V_{\rm mag} < 16$), while the percentage declines for fainter stars, particularly closer to the center where crowding problems are worse. Once we have masked the 3% brightest stars, we measure integrated light by calculating the number of counts per pixel in various annuli using the biweight, a statistically robust estimator (Beers et al. 1990). As discussed in detail in NG06, this appears to be the optimal way to extract a density profile for stars with mass at or around the turnoff mass for an evolved cluster. The choice of the sizes for the annuli is a tradeoff between obtaining the highest spatial resolution and obtaining the least noisy profile possible.

The second method we use to measure density profiles is star counts. From a star list, we construct a star count profile in the same annuli where we measure integrated light. This is done by estimating the number of stars per unit area, where every star has the same weight. As mentioned above, it is well known that in crowded field photometry, fainter stars are detected with decreased efficiency. The exact completeness fraction for a given brightness at a given radius depends on the specific shape of each profile. Given that the surface brightness profiles are dominated by the brightest stars, we measure star count profiles only for the stars brighter than a given magnitude for each cluster, since this is the only way to make a meaningful comparison between the two methods. In order to obtain formally correct star count profiles from images, one must calculate the correct completeness correction factor for each brightness group in each image, which is very time consuming and outside the scope of this work. Uncorrected star counts have been used to measure density profiles for star clusters recently (e.g., Lanzoni et al. 2007), so we feel that it is relevant to compare to such profiles. For the models containing IMBHs, the brightness cutoff always corresponds to 16 mag (slightly fainter than the turnoff point, equivalent to stars with 0.8 $M_{\odot}$); for the non-IMBH models, the limiting magnitude changes with evolution time and is brighter than 16 mag for every case except the most evolved case at 16 Gyr. We use these limiting magnitudes to calculate a star count profile from the original input list, as opposed to the detected list, and we call this the "N-body profile." We compare our measured profiles against this N-body profile, which can be thought of as the "true" profile of the cluster, since it comes straight out of the entire model data set. The precise limiting magnitude for each model is taken as the one for which the surface brightness profile matches the N-body profile in the region outside the core radius.

We note that every simulated cluster, with and without IMBHs, shows mass segregation, as can be seen in Figure 2 where we compare profiles obtained from the input list for various brightness groups. As expected, the profiles for the brightest stars are more concentrated than for the intermediate and faintest groups. The faintest group almost always shows flat central densities, except for the case containing a 2.0% $M_{\rm TOT}$

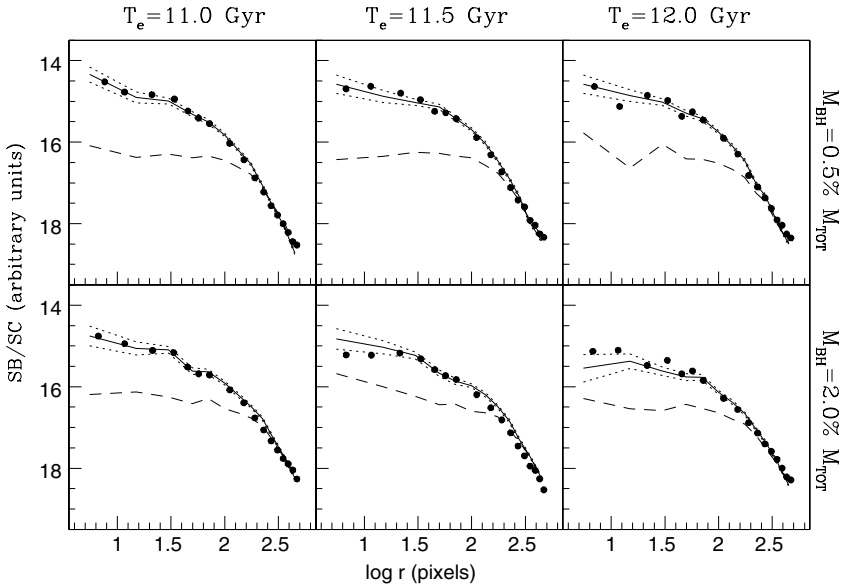

Figure 3. Surface brightness and star count profiles for models with IMBHs of 0.5% and 2.0% $M_{\rm TOT}$ at evolution times of 11.0, 11.5, and 12.0 Gyr. The solid line is the *N*-body profile, the dotted lines mark the Poisson error for the *N*-body profile, the dashed line is the star count profile, and the filled points are the measured photometric points. The vertical scale is arbitrary. Uncorrected star counts underestimate central surface densities by a factor of 2–5, while photometric measurements are better suited to determine density profile for crowded fields, they always lie within the errors of the *N*-body profile.

IMBH. As explained above, the solid lines in this figure are taken as our "*N*-body" profile for every model.

We compare the measured surface brightness and star count profiles with the *N*-body profiles. This is shown in Figure 3 where we present three profiles for models with IMBHs of 0.5% and 2.0% $M_{\rm TOT}$ at different evolution times of 11.0, 11.5, and 12.0 Gyr. The limiting magnitude for the *N*-body profile and the measured star count profile is always the same. We note that the uncorrected star count profiles always underestimate the density for the central regions, including at and around the core radius, while all three profiles agree very well at large radii. The *N*-body profile is sometimes noisy at the center, which is expected due to the small numbers of bright stars in that region. We show the Poisson noise region for the *N*-body profile. As can be seen, for every case, the integrated light profile follows the *N*-body profiles very well at $r > 30''$, and is as smooth as the *N*-body profile inside the core. The shape of the surface brightness profile is clearly dominated by the brightest stars, but the masking of the bright stars combined with the background contribution from fainter stars helps to make it smooth. It practically always lies within the Poisson errors for the *N*-body profile.

Once we have obtained the photometric points for each case, we use a smoothing spline (Wahba & Wang 1990) in order to obtain a smooth profile for further analysis. Since we want to measure half-light radii as well as fit King profiles, we need to cover the complete radial extent for the clusters. Given that both surface brightness and star counts agree very well with the *N*-body profile at large radii, we extend the measurements using the *N*-body profile to the complete radial extent of each modeled cluster. We decide to truncate the star counts at the 0.2 pc width annulus for which we no longer detect stars. There might be stars present at larger radii, but we know that they are very few. The lower density limit we use is lower than what one could measure for observed Galactic clusters, where the field population already would dominate the measurements. In the end, we fit a smooth spline to a combination of our measured photometric points for the radial extent of our images, and of the *N*-body profile at larger radii.

5. ANALYSIS

As mentioned in Section 1, two types of photometrical measurements have been proposed as possible diagnostics for the presence of IMBHs in star clusters, the central slope of the density profile, and the r_c/r_h ratio. In this section we explain how we obtain both quantities for our simulated clusters.

The measurement of the half-light radius (r_h) is straightforward once we have the complete smooth profiles. We integrate the light profile to get the total luminosity and take the radius at which the profile contains half the amount of light. The measurement of the core radius is more complicated since there are different definitions and ways to measure it for observations and numerical modeling. In this work, we explore three different ways to measure core radii that are normally used for observed clusters. The first is the one used by Trager et al. (1995) and Harris (1996), whose results are the sources for most studies of large samples of Galactic globular clusters. These catalogs define the core radius as the half-width half-maximum of the radial density profile (r_{ch} from now on). This definition makes the radius resolution dependent when the profiles are not flat toward the center, since the closer to the center we measure, the brighter the central luminosity value becomes. A second definition is the one that comes from fitting a single-mass King profile (King 1962) to the density profile and taking the value of the fit for the core radius (which we call r_{ck}). The third definition is the one used in NG06, called break radius, and defined as the radius of maximum curvature of the density profile (called r_b). It can be understood as the turnover radius.

As can be seen in Figure 4 and Table 2, the agreement between the three radii is good for models with central slopes between 0.05 and −0.05 (i.e., those with flat central cores). As expected, r_{ch} is smaller than the other two radii for models with central cusps. It can also be seen that the King fits agree very well with the observed profiles for models with flat cores, while for the rest, the agreement of the King fit is good only outside the core radius, but the values of r_{ck} and r_b start to diverge. Note

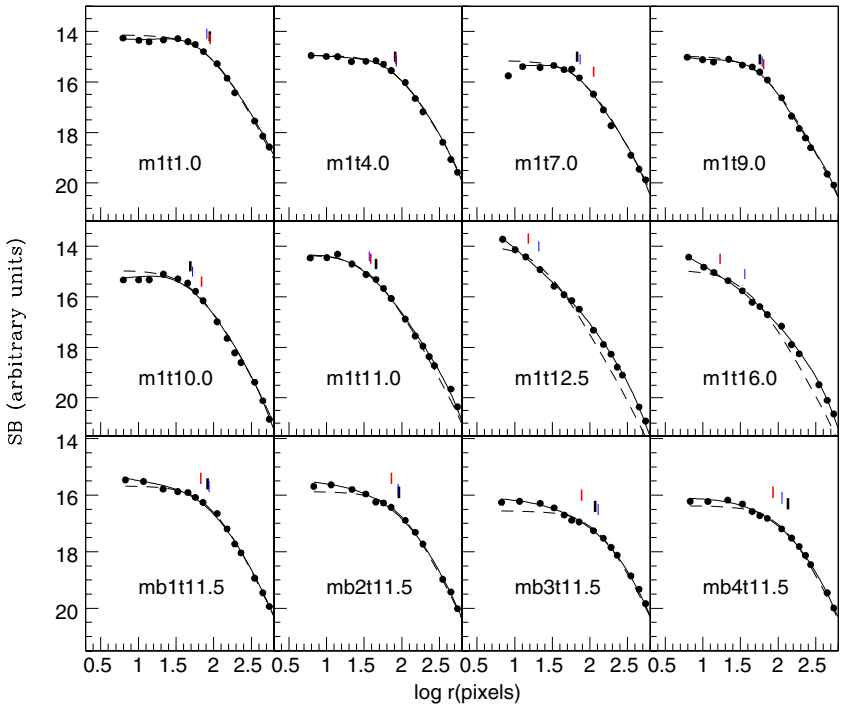

Figure 4. Photometric points for various snapshots of models with and without IMBHs. The solid line is a smooth profile from the data points, the dashed line is a single-mass King fit. The vertical lines mark the different measured radii: black (thickest) is the break radius, blue marks the radius from King fit, and red (thinnest) marks the FWHM core radius.

(A color version of this figure is available in the online journal.)

Table 2
Results

Model	SB Slope	r_b (pc)	r_{ch} (pc)	r_{ck} (pc)	r_h (pc)
m1t1.0	−0.01	1.7	1.7	1.6	7.0
m1t4.0	0.07	1.6	1.6	1.6	5.2
m1t7.0	0.00	1.3	2.2	1.5	5.4
m1t9.0	−0.05	1.1	1.3	1.2	5.5
m1t10.0	−0.09	1.0	1.3	0.0	4.5
m1t11.0	−0.07	0.9	0.8	0.7	4.8
m1t12.5	−1.00	...	0.3	0.4	4.1
m1t16.0	−0.71	...	0.3	0.7	5.4
m2t2.0	0.04	5.4	5.1	5.5	10.8
m2t6.0	−0.05	4.5	4.5	3.8	7.2
m2t8.0	−0.05	2.6	2.0	1.7	5.8
m3t2.0	−0.07	2.9	2.7	4.0	9.0
m3t5.0	0.18	2.2	4.1	3.4	8.9
m3t8.0	−0.11	2.6	2.4	3.3	8.3
m3t11.0	−0.08	2.2	2.2	2.9	8.4
m3t14.0	0.08	1.8	2.3	2.0	7.4
mb1t11.5	−0.18	1.6	1.3	1.7	8.4
mb2t11.0	−0.26	1.8	0.9	1.6	8.8
mb2t11.5	−0.17	1.8	1.4	1.8	8.8
mb2t12.0	−0.18	1.9	1.3	1.8	8.7
mb3t11.5	−0.13	2.3	1.5	2.5	10.3
mb4t3.0	−0.20	2.3	0.7	1.4	7.0
mb4t6.0	−0.45	2.0	0.7	1.8	8.3
mb4t9.0	−0.07	2.0	1.8	2.2	8.7
mb4t11.0	−0.28	1.9	0.9	2.2	10.4
mb4t11.5	−0.07	2.6	1.7	2.2	9.6
mb4t12.0	−0.19	1.7	1.5	2.2	10.1
mb5t11.3	−0.17	1.8	1.3	1.7	8.8
mb5t11.8	−0.16	2.0	1.1	1.6	8.6
mb5t12.0	−0.39	2.1	0.7	1.4	8.4

that the King fit does not describe the profile well toward the center. For models m1t12.5 and m1t16.0, the profiles are so steep that we cannot measure a reliable minimum of curvature (r_b). The King fit for these cases is a bad match for the entire radial extent, so, even though one can formally obtain a value for r_{ck} and r_{ch}, neither of them provide meaningful information about the density profile. For the cases in which we have three close snapshots, we note that the deviation between the different radial measurements is of order 10% for r_b, 20% for r_{ch}, and 5% for r_{ck}, but the deviation between the three different types of core radii is larger.

The central surface brightness slope is obtained by calculating the derivative of the smooth profile inside the core radius. This derivative is constant for $r < r_b$. It is worth mentioning that the value is the same when we measure the slope of a linear fit to the photometric points in the same region. For the couple of very concentrated cases, models m1t12.5 and m1t16.0, where we cannot reliably measure a break radius, we take the central values of the derivative as the slope.

If we try to use completeness-uncorrected profiles instead of light profiles the value for r_h, r_b, and r_{ck} does not change much, since it is the shape of the profile inside the core radius that changes, but not the turnover radius. r_{ch}, on the other hand, suffers a larger change since the value of the central density is lower. Obviously, the value of the central slope is very different (flatter in general). If we try to construct a star count profile using only those stars that are detected with close to 100% completeness, there are too few stars left and the profile becomes too noisy in the center to make any meaningful measurements.

Figure 5 shows the fit of single-mass King profiles to model m3t, which contains stellar-mass black holes. It can be seen that the fits are significantly more noisy in the center than those for models m1t and m2t, which is most likely due to

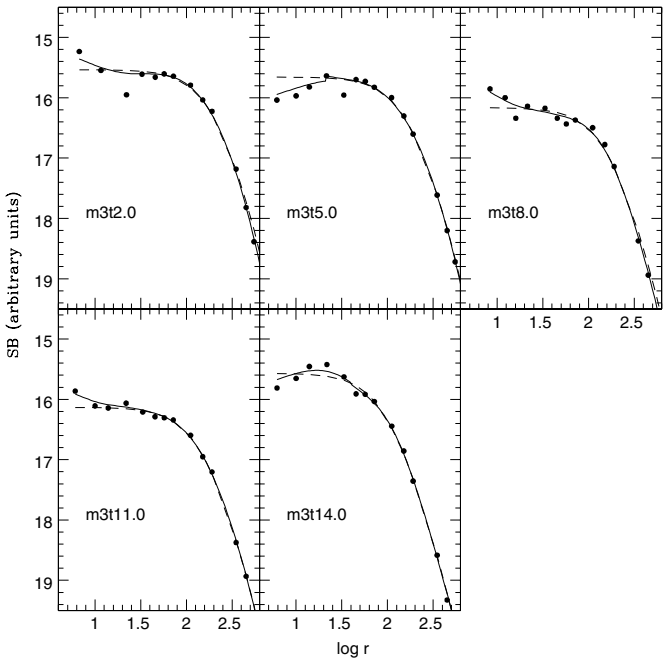

Figure 5. Photometric points for various snapshots of models without IMBHs but containing stellar-mass black holes. The solid line is a smooth profile from the data points, the dashed line is a single-mass King fit.

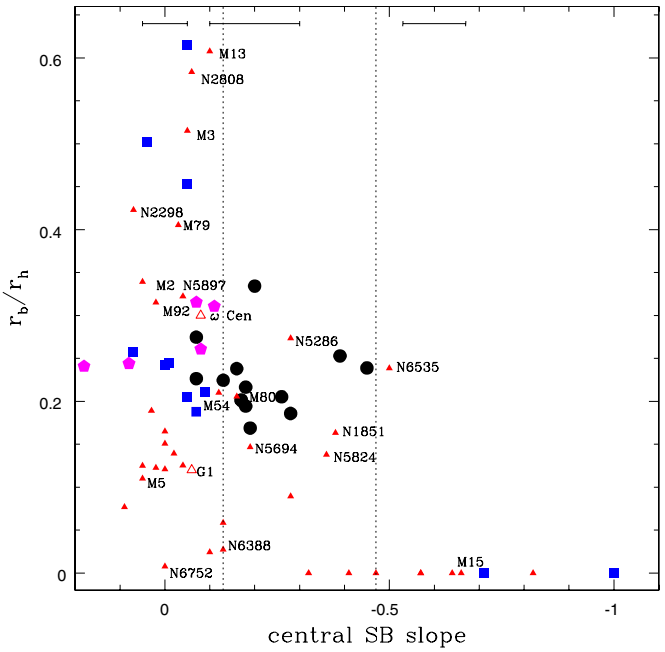

Figure 6. Central surface brightness slope vs. the ratio of r_b/r_h. The full circles mark the location of models containing IMBHs, the full squares are for models without an IMBH, and the full pentagons are for models containing stellar-mass black holes. Representative error bars for the central slopes (NG06) are shown on the top. The full triangles mark the location of 38 Galactic globular clusters, while the open triangles are for G1 and omega Cen. Some individual globular clusters are labeled.

(A color version of this figure is available in the online journal.)

the more stochastic heating of the cluster by a few black holes as compared to a core of neutron stars and white dwarfs. Table 2 shows that the derived photometric parameters are nevertheless still within the range seen for those of clusters without stellar-mass black holes, in particular the central surface brightness slopes are still all below -0.12.

Once we have central surface brightness slopes and r_c/r_h measurements for every modeled cluster we proceed to plot each point on a slope versus r_c/r_h plane. We create a plane for each of the three measured radii. We find that using r_{ck} or r_b gives very similar results, while using r_{rh} does not give meaningful constraints for clusters without flat central light profiles, so we exclude this quantity from further analysis. In Figures 6 and 7 we show the location of our models on the slope versus r_b/r_h and r_{ck}/r_h planes, respectively. The models span a range of central slopes from 0.18 to -1.00, but the only models that have slopes steeper than -0.5 are those that have achieved core-collapse, while the steepest slope for a model containing an IMBH is -0.45. As shown in Figures 6 and 7, there are two models containing an IMBH that present a flat central core (model mb4t9.0 and mb4t11.5), otherwise, only the models containing IMBHs show shallow central cusps. Models without IMBHs show either a flat central slope or steep central cusps. Regarding the r_b/r_h ratio, the cases that have not reached core-collapse and started from a King model with $W_0 = 7$ lie within a narrow range between 0.15 and 0.35 and there is no clear distinction between these cases and those containing IMBHs in this respect. The cases that clearly separate toward large r_c/r_h are those that started from King models with $W_0 = 5$. The models containing stellar-mass black holes lie close to the first group, but have larger r_b/r_h values. The two core-collapsed cases are placed at $r_b/r_h = 0$, since we cannot formally measure a break radius for them. For the r_{ck}/r_h case, the actual values change, but the behavior is similar. The only group of models that clearly separates from the rest in both plots is that with very steep central slopes and non-detectable turnover radius, which correspond to

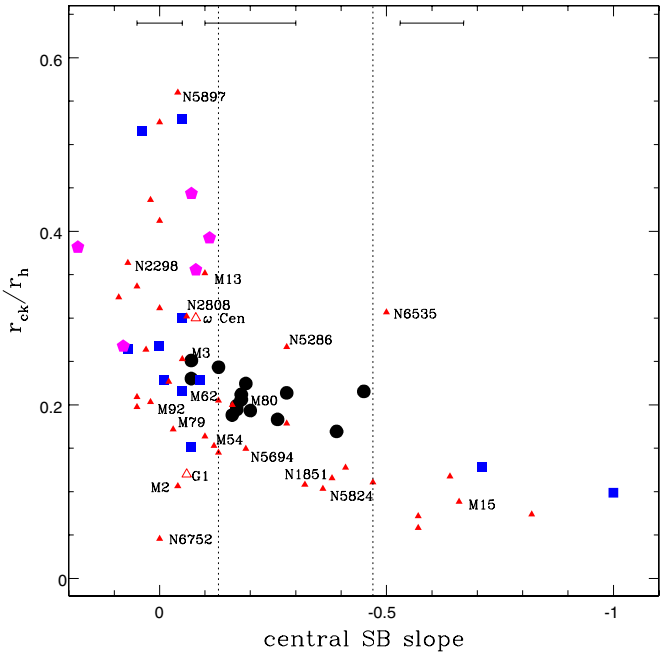

Figure 7. Central surface brightness slope vs. the ratio of r_{ck}/r_h. The filled circles mark the location of models containing IMBHs, the filled squares are for the models without an IMBH, and the full pentagons are for models containing stellar-mass black holes. As in the previous figure, representative error bars for the central slopes (NG06) are shown on the top, the full triangles mark the location of 38 Galactic globular clusters, while the open triangles are for G1 and omega Cen. Some individual globular clusters are labeled.

(A color version of this figure is available in the online journal.)

clusters that do not contain IMBHs and have undergone core-collapse.

We overlay on both planes all the Galactic clusters in NG06, plus omega Centauri and G1. For G1 we measure the central slope using the profile in Gebhardt et al. (2005), while r_c and r_h values come from the analysis of Ma et al. (2007). The first thing to note is that the Galactic clusters occupy a larger area in the plane than the modeled ones. The two clusters for which there are kinematical indications of hosting an IMBH, G1 and omega Centauri have central density slopes shallower than -0.1, and their r_c/r_h values are different. Omega Centauri and G1 sit near the locus of our models, but both of them have more extreme values of r_c/r_h than the models with IMBHs. Very concentrated clusters, like M15, which are assumed to have undergone core-collapse, do lie very close to the models without IMBHs and long evolutionary times. It should be noticed that some individual Galactic clusters change location from one plane to the other.

6. DISCUSSION AND CONCLUSIONS

M15 was the first cluster for which the presence of a central massive black hole was kinematically investigated, mainly due to its concentrated central profile. It was only later when it became clear that a projected steep central cusp is not the expected behavior for a star cluster containing a black hole. This stresses the need to develop better diagnostics to discriminate suitable candidates for detailed kinematical measurements when looking for IMBHs. In this paper, we have created realistic synthetic images from *N*-body models of star clusters with and without IMBHs. We have analyzed these images in the same way we analyze *HST* data for a sample of Galactic globular clusters and we compare both data sets. We explore two quantities as possible diagnostic tools for the presence of black holes: the central logarithmic slope of the surface brightness profile and the ratio of core radius to half-light radius. We find that the r_c/r_h ratio cannot discriminate between models with and without black holes, as Hurley (2007) already found, but that the central logarithmic slope can. *N*-body clusters without IMBHs show either flat central cores or steep cusps if they have undergone core-collapse, while clusters containing IMBHs show shallow central cusp for all except two cases.

We want to emphasize that when dealing with density profiles of star clusters, saying "core radius" alone is not enough, one has to specify how that radius is measured in order to compare its value to models or other observations. Historically, the definition that we call r_{ch} is the most popular one, but we show here that this definition is only useful for clusters whose profiles have a flat central core. When the profiles have central slopes different from zero, r_{ck} or r_b appear to be more suitable, although they can differ by up to a factor of two for the same cluster. For density profiles with a flat central core and clear turnovers, all three definitions mark practically the same radius.

There are various ways in which our *N*-body simulations are idealized compared to Galactic globular clusters. First, the number of stars and the central densities are lower than for real clusters. Increasing both quantities would increase the relaxation time, which in turn would increase the evolutionary times. Including the presence of binaries could change not only the timescales but also the nature of the core contraction and expansion. Also, our analysis comes from images with a limited amount of signal to noise (a combination of number of stars and fiducial distance). It is likely that the comparisons would be more meaningful using images with a larger number of stars. These issues have to be kept in mind when comparing to observed globular clusters. Despite the idealizations in the models, the span of r_c/r_h and central slope values seems to generally agree between our models and observed clusters. We note that the agreement between the two models that have undergone core-collapse and the observed clusters that are suspected of having undergone the same process is very good. Having simulations with a larger number of stars would allow to analyze snapshots closer in time to fully explore the process of core-collapse. There are some areas of Figures 6 and 7 containing observed clusters that our models do not populate. As mentioned in Section 1, a variety of heating mechanisms have been proposed for star clusters in recent years. Some of them, like mass loss or white dwarf kicks should affect most clusters; while others like tidal shocking or primordial binaries depend on the structure and evolution history of each cluster. A combination of including some of these heating mechanisms and starting from a larger variety of configurations (a larger range of initial W_0) would likely produce a better agreement between models and observations.

Our results are in contrast with those of Vesperini & Trenti (2010) since they find a number of models that present central shallow cusps without containing black holes. We think the reason for the difference between their result and ours lies on a combination of two things: on one hand, their models contain about 10% of the number of stars our models have. On the other hand, they count main-sequence stars, which we find to be detected with a large degree of incompleteness in realistic analysis, particularly in the center of rich clusters. Thus, we are tracing a different subset of stars when measuring density profiles. We believe that the lower numbers of stars in their models produce noisier profiles that in turn can show shallow cusps due to fluctuations in the photometric points. This is illustrated by the fact that as soon as they use more particles (64K runs with combined snapshots), their central slopes before core-collapse times converge to shallower values consistent with the ones we find for models without black holes.

It is clear from Figures 6 and 7 that a division can be made between clusters with and without IMBHs using only one of the two quantities that we have explored, the central logarithmic slope of the surface brightness profile. The r_c/r_h ratio cannot distinguish between cases with and without black holes, only between clusters that have undergone core-collapse and the rest. Clusters that have achieved core-collapse separate cleanly from the rest in both indicators, which leads to the exclusion of very concentrated clusters, like M15, as candidates for hosting an IMBH. None of our models reproduce central slopes between 0.5 and 0.65 and we observe a few Galactic globular clusters with those slopes. Since we are not able to follow the details of the evolution right before core-collapse due to the time intervals between snapshots, we cannot rule out the possibility that clusters in this stage could have intermediate slopes Even if clusters undergo such a phase, it is expected to be only for a very short time. Two of the 14 models containing IMBHs do not show a clear central shallow cusp. Even though it is impossible to draw statistical conclusions from such a small sample, we can say that the absence of shallow cusp does not imply the absence of a central black hole. Therefore, some clusters with shallow cores might still be interesting candidates to follow up with kinematics. Finally, clusters with central slopes between -0.1 and -0.45 are clear candidates for harboring central black holes since we can only reproduce shallow central slopes by including IMBHs. We conclude that the central logarithmic surface brightness slope appears to be

a good diagnostic tool for choosing star cluster candidates for harboring IMBHs.

H.B. acknowledges support from the German Science foundation through a Heisenberg Fellowship and from the Australian Research Council through Future Fellowship grant FT0991052. The authors thank the hospitality of the Kavli Institute for Theoretical Physics at UCSB, as well as the organizers of the "Formation and Evolution of Globular Clusters" program there. We also thank the anonymous referee for making useful suggestions that helped improve the manuscript.

REFERENCES

Aarseth, S. J. 1999, PASP, 111, 1333
Anderson, J., & van der Marel, R. P. 2010, ApJ, 710, 1032
Bahcall, J. N., & Wolf, R. A. 1976, ApJ, 209, 214
Bastian, N., Gieles, M., Goodwin, S. P., et al. 2008, MNRAS, 389, 223
Baumgardt, H., Heggie, D. C., Hut, P., & Makino, J. 2003a, MNRAS, 341, 247
Baumgardt, H., Hut, P., Makino, J., McMillan, S., & Portegies Zwart, S. 2003b, ApJ, 582, L21
Baumgardt, H., & Kroupa, P. 2007, MNRAS, 380, 1589
Baumgardt, H., Makino, J., & Ebisuzaki, T. 2004a, ApJ, 613, 1133
Baumgardt, H., Makino, J., & Ebisuzaki, T. 2004b, ApJ, 613, 1143
Baumgardt, H., Makino, J., & Hut, P. 2005, ApJ, 620, 238
Baumgardt, H., Makino, J., Hut, P., McMillan, S., & Portegies Zwart, S. 2003c, ApJ, 589, L25
Beers, T. C., Flynn, K., & Gebhardt, K. 1990, AJ, 100, 32
Casertano, S., & Hut, P. 1985, ApJ, 298, 80
Cohn, H. 1980, ApJ, 242, 765
Davis, D. S., Richer, H. B., King, I. R., et al. 2008, MNRAS, 383, L20
Drukier, G. A. 1995, ApJS, 100, 347
Drukier, G. A., Bailyn, C. D., Van Altena, W. F., & Girard, T. M. 2003, AJ, 125, 2559
Drukier, G. A., Fahlman, G. G., & Richer, H. B. 1992, ApJ, 386, 106
Dull, J. D., Cohn, H. N., Lugger, P. M., et al. 1997, ApJ, 481, 267
Ferraro, F. R., Possenti, A., Sabbi, E., et al. 2003, ApJ, 595, 179
Fregeau, J. M. 2008, ApJ, 673, L25
Fregeau, J. M., Richer, H. B., Rasio, F. A., & Hurley, J. R. 2009, ApJ, 695, L20
Gao, B., Goodman, J., Cohn, H., & Murphy, B. 1991, ApJ, 370, 567
Gebhardt, K., Rich, R. M., & Ho, L. C. 2005, ApJ, 634, 1093
Gebhardt, K., Richstone, D., Tremaine, S., et al. 2003, ApJ, 583, 92
Gerssen, J., van der Marel, R. P., Gebhardt, K., et al. 2002, AJ, 124, 3270
Gerssen, J., van der Marel, R. P., Gebhardt, K., et al. 2003, AJ, 125, 376
Harris, W. E. 1996, AJ, 112, 1487
Hurley, J. R. 2007, MNRAS, 379, 93
Hurley, J. R., Pols, O. R., & Tout, C. A. 2000, MNRAS, 315, 543
Irwin, J. A., Brink, T. G., Bregman, J. N., & Roberts, T. P. 2010, ApJ, 712, L1
King, I. 1962, AJ, 67, 471
King, I. R. 1966, AJ, 71, 276
Kochanek, C. 1992, AJ, 385, 604
Kroupa, P. 2001, MNRAS, 322, 231
Lanzoni, B., Dalessandro, E., Ferraro, F., et al. 2007, ApJ, 668, L139
Lugger, P. M., Cohn, H. N., & Grindlay, J. E. 1995, ApJ, 439, 191
Lützgendorf, N., Kissler-Patig, M., Noyola, E., et al. 2011, A&A, 533, 36
Ma, J., de Grijs, R., Chen, D., et al. 2007, MNRAS, 376, 1621
Maccarone, T. J., Kundu, A., Zepf, S. E., & Rhode, K. L. 2007, Nature, 445, 183
Mackey, A. D., Wilkinson, M. I., Davies, M. B., & Gilmore, G. F. 2008, MNRAS, 386, 65
Magorrian, J., Tremaine, S., Richstone, D., et al. 1998, AJ, 115, 2285
Matsumoto, H., & Tsuru, T. G. 1999, PASJ, 51, 321
Matsumoto, H., Tsuru, T. G., Koyama, K., et al. 2001, ApJ, 547, L25
McCrady, N., Gilbert, A. M., & Graham, J. R. 2003, ApJ, 596, 240
McNamara, B. J., Harrison, T. E., & Baumgardt, H. 2004, ApJ, 602, 264
Noyola, E., & Gebhardt, K. 2006, AJ, 132, 447
Noyola, E., & Gebhardt, K. 2007, AJ, 134, 912
Noyola, E., Gebhardt, K., & Bergmann, M. 2008, ApJ, 676, 1008
Pfahl, E., Rappaport, S., & Podsiadlowski, P. 2002a, ApJ, 573, 283
Pfahl, E., Rappaport, S., Podsiadlowski, P., & Spruit, H. 2002b, ApJ, 574, 364
Pooley, D., & Rappaport, S. 2006, ApJ, 644, L45
Stetson, P. B. 1987, PASP, 99, 191
Strohmayer, T. E., & Mushotzky, R. F. 2003, ApJ, 586, L61
Trager, S. C., King, I. R., & Djorgovski, S. 1995, AJ, 109, 218
Trenti, M., Ardi, E., Mineshige, S., & Hut, P. 2007, MNRAS, 374, 857
Ulvestad, J. S., Greene, J., & Ho, L. 2007, ApJ, 661, L151
van den Bosch, R., de Zeeuw, T., Gebhardt, K., Noyola, E., & van de Ven, G. 2006, ApJ, 641, 852
van der Marel, R. P., & Anderson, J. 2010, ApJ, 710, 1063
Vesperini, E., & Chernoff, D. F. 1994, ApJ, 431, 231
Vesperini, E., & Trenti, M. 2010, ApJ, 720, 179
Wahba, G., & Wang, Y. 1990, Commun. Stat. A: Theory Methods, 19, 1685
Zepf, S. E., Stern, D., Maccarone, T. J., et al. 2008, ApJ, 683, L139